Strong biological carbon uptake and carbonate chemistry associated with dense shelf water outflows in the Cape Darnley polynya, East Antarctica

Kan Murakami[a], Daiki Nomura[a, b, c, d] *, Gen Hashida[e], Shin-ichiro Nakaoka[f], Yujiro Kitade[g], Daisuke Hirano[c, h], Toru Hirawake[a, c], and Kay I. Ohshima[c, h]

[a] *Faculty of Fisheries Sciences, Hokkaido University, 3-1-1, Minato-cho, Hakodate, Hokkaido 041-8611, Japan.*

[b] *Field Science Center for Northern Biosphere, Hokkaido University, 3-1-1, Minato-cho, Hakodate, Hokkaido 041-8611, Japan.*

[c] *Arctic Research Center, Hokkaido University, Kita 21, Nishi 11, Kita-ku, Sapporo, Hokkaido 001-0021, Japan.*

[d] *Global Station for Arctic Research, Global Institution for Collaborative Research and Education, Hokkaido University, Kita 8, Nishi 5, Kita-ku, Sapporo, Hokkaido 060-0808, Japan.*

[e] *National Institute of Polar Research, 10-3 Midori-cho, Tachikawa, Tokyo 190-8501, Japan.*

[f] *National Institute for Environmental Studies, 16-2 Onogawa, Tsukuba, Ibaraki 305-8506, Japan.*

[g] *Tokyo University of Marine Science and Technology, Tokyo 108-8477, Japan.*

[h] *Institute of Low Temperature Science, Hokkaido University, Kita 19, Nishi 8, Kita-ku, Sapporo, Hokkaido 060-0819, Japan.*

*Corresponding author.

Email address: daiki.nomura@fish.hokudai.ac.jp (D. Nomura) (Field Science Center for Northern Biosphere, Hokkaido University, 3-1-1, Minato-cho, Hakodate, Hokkaido 041-8611, Japan)

Abstract

Formation of dense shelf water (DSW) in coastal polynyas (open water or thin sea-ice cover) in the sea-ice zone around Antarctica supplies Antarctic Bottom Water (AABW) through overflow down the continental slope. In coastal polynyas, atmospheric carbon dioxide (CO_2) is absorbed by the ocean in the early spring because of active primary production, and DSW formation is an important process for transporting this carbon from the sea surface to the deep ocean. However, there have been few quantitative evaluations of carbon consumption by active primary production and transport in coastal polynyas. Here, we examined the carbon dynamics in the Cape Darnley polynya (CDP), East Antarctica during austral summer 2009, by using carbonate system parameters combined with oceanographic mooring data. The partial pressure of CO_2 in the CDP surface water was lower than that of the atmosphere and the mean and standard deviation of sea−air CO_2 flux was estimated as -6.5 ± 6.9 mmol C m^{-2} d^{-1} (a negative value indicates absorption of atmospheric CO_2 by the ocean). Vertical profiles of dissolved inorganic carbon (DIC) concentration showed that concentrations in the bottom layer near the ocean floor were lower (by about 20 μmol kg^{-1}) than those in the ambient water (e.g., modified Circumpolar Deep Water, mCDW). The low-DIC in the shelf water was maintained by the strong biological uptake of carbon imported from high-DIC mCDW within the water column. Therefore, low-DIC DSW overflowed down the continental slope, and low-DIC concentrations were maintained through an export

pathway to the continental shelf. The annual production of dissolved organic carbon and particulate organic carbon on the shelf was estimated as 0.7×10^{11}–1.5×10^{11} mol C using the data for the DIC of DSW and current velocity data from a mooring in the CDP. Our results provide quantitative estimates for and the potential role of carbon consumption by the active primary production and carbon transport by dense water formation in Antarctic coastal polynyas.

Keywords: Carbon dioxide, primary production, carbon transport, dense water formation, gas exchange, polynya, Cape Darnley, Southern Ocean

Highlight

1. Strong biological carbon uptake in the Cape Darnley polynya

2. A Box-model reveals the carbon transport accompanying the outflow of DSW in the Cape Darnley polynya

3. Annual DIC transport from the surface to the deep layer is negative in the Cape Darnley polynya

1. Introduction

The ocean mitigates global warming by absorbing carbon dioxide (CO_2) from the atmosphere and sequestering CO_2 in the deep ocean. The Southern Ocean in particular plays an important role in absorbing atmospheric CO_2 and acts as a CO_2 sink (Sabine et al., 2004; Sallée et al., 2012). In the major CO_2 sink region in the Southern Ocean between 30°S and 50°S, the partial pressure of CO_2 (pCO_2) in the surface water becomes low relative to that in the atmosphere because of the active utilization of dissolved inorganic carbon (DIC) by phytoplankton in the surface water in summer (Takahashi et al., 2012). However, in the areas south of 50°S, the CO_2 source/sink

conditions vary seasonally over a wide range of pCO_2 in the surface waters. Takahashi et al. (2012) have indicated that the areas south of 50°S act as a small CO_2 sink averaged over the year, and Metzl et al. (2006) have indicated a CO_2 source in winter and this is supported by recent results based on autonomous biogeochemical floats leading to an annual CO_2 source at high latitudes (Gray et al., 2018). Lenton et al. (2013) show that the region between 58−78°S is actually a small source of CO_2 to the atmosphere, although interestingly there is some disagreement when they compare various modelling approaches. Landschützer et al. (2015) use a neural network-based approach to produce a new estimate of the global oceanic carbon sink, which Gray et al. (2018) then use to compare their seasonal observational results from biogeochemical profiling floats in the Southern Ocean.

In winter, the Southern Ocean around Antarctica is covered by sea ice (Comiso, 2010). On the other hand, coastal polynyas—areas with thin ice or open water—are areas of intense sea-ice production (Tamura et al., 2008). When sea ice is formed, high-salinity brine is rejected from the sea ice to the underlying water (Wakatsuchi and Ono, 1983), creating dense seawater. This dense water sinks into the deep ocean, and includes any CO_2 absorbed from the atmosphere. This process is thought to be an important system for transporting and sequestering atmospheric CO_2 to the deep ocean and seems to occur most efficiently in coastal polynyas, where sea ice is continuously carried away from the coast by the wind and ocean currents (Nomura et al., 2006; Rysgaard et al., 2007; Roden et al., 2016). Normally, when there is sea ice covered with snow, very little sunlight reaches below the sea ice; but this does not happen in the polynyas, so the ocean surface layer is exposed to sunlight. This stimulates the biological utilization of CO_2 in the surface water (e.g., Arrigo and Van Dijken, 2003) during a sufficient supply of nutrients. As a result, the pCO_2 in the polynya surface water is reduced with respect to the atmosphere, allowing absorption of atmospheric CO_2 into the ocean (DeJong and Dunbar, 2017).

Dense shelf water (DSW) forms on the continental shelf through brine rejection during sea-ice formation and through interactions between the ocean and ice-shelf. Figure 1 is a schematic illustration of the water mass structure in the coast of Antarctica. The

outflow of DSW to the deep ocean creates Antarctic Bottom Water (AABW), which is the main driving source for global overturning circulation (Orsi et al., 1999). Recently, a research group from Japan has shown that DSW forms and sinks, making AABW, in the Cape Darnley polynya (CDP), East Antarctica (Ohshima et al., 2013). The bottom water derived from this area is called Cape Darnley Bottom Water (CDBW), accounting for 13−30% of the total amount of bottom water formed in the Atlantic sector of the Southern Ocean (Williams et al., 2016). Other physical processes occur in this area, such as subduction and mixing of DSW with ambient water (Ohshima et al., 2013; Hirano et al., 2015). In addition, there is summer production of AABW (Hirano et al., 2015). The interaction between these physical and biological processes is an important component of the carbon cycle in the Southern Ocean. However, there are few observations in the biogeochemical field associated with the carbon transport processes accompanying the outflow of DSW in this area (Roden et al., 2016).

AABW is also produced in the Mertz Polynya of East Antarctica. Here it has been reported that CO_2 is transported to the deep sea along with the outflow of DSW (Shadwick et al., 2014). Shadwick et al. (2014) have shown that it is important to understand carbon cycling in the coastal polynya because of the uptake of anthropogenic CO_2 and transport of organic carbon to the deep layer through seasonal modification of DSW. However, field observations are limited, and there are not enough data to discuss carbon cycling in the coastal polynya. Although the amount of DSW produced in the CDP has been clarified (Ohshima et al., 2013; Hirano et al., 2015), there are only a few descriptions of the vertical carbonate chemistry or estimates of carbon transport from the surface to the deep layer (Roden et al., 2016).

In this paper, we describe the carbonate chemistry and carbon cycling in the CDP. In particular, we estimate the carbon transport by DSW outflow and ventilation of AABW, incorporating the characteristics and changes in vertical distributions of biogeochemical properties, and mooring data. We show that sea-surface water absorbs CO_2 from the atmosphere and then transports it into the deep ocean. Furthermore, we use a two-box model to analyze the biological uptake of carbon and carbon balance between the

coastal polynya and the offshore area.

2. Materials and methods

We sampled from the R/V *Umitaka Maru* in the Cape Darnley polynya in the Southern Ocean (66−68°S, 67−71°E) from 22 to 27 January 2009 (Fig. 2). Vertical profiles of temperature, salinity, and dissolved oxygen (DO) were measured with a conductivity-temperature-depth (CTD) probe (SBE 911 plus, Sea-Bird Electronics, Bellevue, WA, USA) and DO sensor (SBE 43, Sea-Bird Electronics, Bellevue, WA, USA). We also collected seawater samples during the cruise to calibrate the salinity and DO sensors in the respective casts. Based on the postcruise calibration, the accuracy levels are 0.001 °C for temperature and 0.002 for salinity. The DO of the bottled samples was measured by the Winkler method (Strickland and Parsons, 1968) and used for the DO-sensor calibration. Precision is ±0.1 mL L^{-1} for DO. Seawater samples were collected vertically in rosette-mounted 2500-mL Niskin bottles (Ocean Test Equipment, Inc., Lauderdale, FL, USA).

Seawater was sampled into a 250-mL amber glass vial (Maruemu Co., Ltd., Osaka, Japan) for the determination of dissolved inorganic carbon (DIC). Immediately after DIC sampling, saturated mercuric chloride ($HgCl_2$) solution (50 μL) was added to stop biological activity, and the vial was sealed with a greased glass stopper. DIC was determined by coulometry using a coulometer (Johnson, 1992). Samples for chlorophyll *a* (chl.*a*) measurement were immediately filtered through 25-mm Whatman GF/F filters and the filters were stored in a deep freezer (−80 °C) until analysis (Suzuki and Ishimaru, 1990). Chl.*a* concentrations were determined by fluorometry (model 10AU fluorometer; Turner Designs, Inc., Sunnyvale, CA). Chl.*a* sampling was conducted only at station (St.) 7 (Fig. 2) near the surface (0−33 m).

The precision of DIC analysis from duplicate determinations was within ± 0.1%. DIC measurements were calibrated by using the reference sea-water materials (Batch AG;

KANSO Technos Co., Ltd, Osaka, Japan) traceable to the certified reference material distributed by A. G. Dickson of Scripps Institution of Oceanography. We applied multiple linear regression (MLR) to complement the limited DIC samples and evaluate the vertical distribution of DIC concentrations in detail. We used Eq. 1 to calculate DIC concentrations by MLR.

$$DIC_{MLR} = a \cdot \theta + b \cdot S + c \cdot DO + d \quad (1),$$

where θ (potential temperature), S, and DO are explanatory variables from the CTD measurements, and a, b, c, and d are partial regression coefficients. Figure 3 shows the relationship between DIC_{MLR} and DIC_{obs}. We obtained a high correlation ($r^2 = 0.87$, $P < 0.0001$, $n = 30$) between the two sets of results. We could complement our measured DIC values with estimates from MLR within the range of the standard deviation (± 5.8 μmol kg^{-1}).

During the cruise, sea surface temperature (SST) and salinity (SSS), and the pCO_2 in surface water were evaluated through the onboard underway water monitoring system (Inoue and Ishii, 2005; Nakaoka et al., 2009). SST and SSS were measured continuously with a conductivity-temperature (CT) sensor (Falmouth Scientific, Inc., Cataumet, MA, USA). The accuracy of temperature and salinity were ±0.005 °C and ±0.001, respectively. Seawater samples were collected in order to calibrate the conductivity sensor. The CO_2 concentration (mole fraction of CO_2 in dry air; xCO_2) was measured quasi-continuously in air equilibrated with seawater using an automated CO_2 measuring system (Nippon ANS Co. Ltd., Tokyo, Japan). This system included a unit for removing water vapor from sample air: a chemical desiccant column containing $Mg(ClO_4)_2$ and an electric dehumidifier. Seawater was pumped continuously from a depth of about 10 m and introduced into a shower-type equilibrator (Inoue and Ishii, 2005). A non-dispersive infrared gas analyzer (NDIR) (Model 800, LI-COR, Inc., Lincoln, NE, USA) was used as the detector for measuring CO_2. The analyzer was

calibrated every hour with four CO_2 standards (200, 266, 320 and 400 ppm) traceable to the World Meteorological Organization mole fraction scale (Inoue and Ishii, 2005). For measurements of atmospheric CO_2 concentration, air samples were pumped through a polytetrafluoroethene (PTFE) tube from the ship's mast and introduced to the CO_2 analyzer every six minutes. pCO_2 was calculated from xCO_2 taking into account the saturated water vapor pressure and atmospheric pressure. The precision of pCO_2 measurements was less than 2 μatm, as estimated on the basis of the uncertainty from the rise in seawater temperature between the surface and the NDIR analyzer (1 μatm). The rise in seawater temperature between the surface and the equilibrator was typically about 1.7 °C, and the effect of the temperature increase on the measured pCO_2 was corrected using the iso-chemical temperature dependence of pCO_2 given by Copin-Montegut (1988).

The sea–air CO_2 flux was calculated using Eq. 2:

$$F_{sea\text{-}air} = k\,\alpha\,\Delta pCO_2 \qquad (2),$$

where k is the gas transfer velocity (Wanninkhof et al., 2013), α is the CO_2 solubility (Weiss, 1974), and ΔpCO_2 is the difference in pCO_2 between the sea surface and the atmosphere. The gas transfer velocity was computed using measured wind speeds from the ship's mast. In this paper, sea–air gas flux was estimated on the assumption that the sea surface in the polynya was 100% open water with no sea-ice cover.

Ocean color chl.*a* of the moderate resolution imaging spectroradiometer (MODIS) on Aqua satellite were analyzed to derive chl.*a* distribution near our sampling stations. We obtained 8-days level-3 standard mapped image (SMI) of chl.*a* from NASA Ocean Color Web (https://oceancolor.gsfc.nasa.gov). Spatial resolution was 4 km and algorithm of chl.*a* product was OC3 (O'Reilly et al. 2000).

3. Results

3.1. Vertical profiles of temperature, salinity, DO, DIC, and chl.a

In order to define the water masses, we referred to Orsi and Wiederwohl (2009) and Roden et al. (2016), using neutral density (γ_n) (Jackett and McDougal, 1997) and potential temperature. In this study we defined modified Circumpolar Deep Water (mCDW), Antarctic Surface Water (AASW), and modified Shelf Water (mSW), the precursor to AABW. The properties of each water mass are summarized in Table 1, and a schematic illustration of the water mass structure was shown in Figure 1.

We show vertical profiles for each parameter at St. 3 (Fig. 4). In the surface water, the temperature was approximately 0 °C (Fig. 4a) and salinity was the lowest (34.0) of the water column (Fig. 4b). Relatively warm and fresh "summer" water occupied the top surface of the ocean. DO was high in the surface layer (8.9 mL L^{-1}; Fig. 4c), whereas the DIC_{obs} concentration was low (2142 μmol kg^{-1}; Fig. 4d). There was a temperature minimum at 67-m depth (T_{min}, −1.6 °C). This layer is "Winter Water" (WW), which is the remnant of the mixed layer from the preceding late winter. The surface waters were dominated by AASW (γ^n < 28.0 kg m^{-3}) above 200-m depth. Below 200-m depth, mCDW was dominated and there was no CDW (Orsi and Wiederwohl, 2009 and Roden et al., 2016) in our study area (Table 1). Temperature increased up to +0.7 °C (500 m) with depth, and we observed θ > +0.5 °C between depths of 350 and 1100 m. Salinity increased down to 1000-m depth and was as high as 34.7; it then remained almost constant to the bottom layer. DO decreased with depth and was as low as 5.3 mL L^{-1} at 1000-m depth. DIC_{obs} concentration was highest (2253 μmol kg^{-1}) at 1500-m depth. From the middle layer (1500-m depth) to the bottom layer on the slope, temperature decreased slightly to −0.5 °C. DO increased from 5.3 to 6.2 mL L^{-1} from 1500 m to the ocean floor. The DIC_{obs} concentration decreased from 2253 to 2233 μmol kg^{-1} over the same depth range by approximately 20 μmol kg^{-1}. Generally, DIC_{obs} and DIC_{MLR}

concentrations were identical through the water column although there was difference between them at the bottom of layer. The chl.*a* concentration at St. 7 ranged from 2.3 to 3.8 μg L^{-1} from the surface to 16-m depth and from 4.7 to 5.1 μg L^{-1} from 15- to 32-m depth (data not shown).

We prepared north–south sections showing the distribution of physical and biogeochemical parameters (Sts. 1−6) to illustrate latitudinal features (Fig. 5). For each parameter, the vertical structure was roughly similar to the corresponding vertical profile shown in Figure 4. However, there were differences with latitude. We observed high temperature, salinity, and DIC concentrations and low DO between 500 and 1000 m north of 66.9°S. At Sts. 4 and 5, south of 66.9°S, we observed AASW with low temperature, salinity, and DIC concentrations and high DO in the surface layer (100−200 m). This AASW became shallower at St. 6, and modified Shelf Water (mSW) was evident under the AASW. The mSW formed an important structure that led from the shelf edge to the deep layer over the slope (Fig. 5). This structure coincided with the distribution of a neutral density of 28.27.

We mapped the DIC concentration in the bottom layer (5 and 100 m above the bottom) for all stations (Fig. 6). From south to north (from St. 6 to St. 1), DIC concentrations in both layers clearly increased. For example, the bottom DIC concentration was 2227 μmol kg^{-1} at St. 6 and 2257 μmol kg^{-1} at St. 1, an increase of approximately 30 μmol kg^{-1}. This increase was within the same water mass (mSW) extending into deeper water along the slope. At St. 3 there was a large difference between DIC concentrations in the bottom and middle layers, although there was no such difference at St. 1, with almost uniform DIC concentrations from the middle layer to the bottom.

3.2. Surface underway distribution and air-sea CO_2 fluxes

South of 67.0°S, SST decreased to below 0 °C, and SSS decreased to 32.5. North of 67°S, however, SST increased to +2 °C, and SSS rose to 34.0 around 66.5°S (Fig. 7a

and b). Surface-water pCO_2 ($pCO_{2\ sea}$) ranged widely from 172 to 362 μatm and was low with respect to the mean air pCO_2 (approximately 372 μatm). There was a particularly large difference between sea-surface and atmospheric pCO_2 south of 67.0°S. SST, SSS, and $pCO_{2\ sea}$ were all low around the limited ice-edge near the coast (Figs. 2 and 7).

$F_{sea–air}$ calculated from Eq. 2 ranged from −25.1 to −0.2 mmol C m^{-2} d^{-1} (a negative value indicates absorption of atmospheric CO_2 into the sea surface) (Fig. 7d), and the mean and standard deviation of flux was −6.5 ± 6.9 mmol C m^{-2} d^{-1}, indicating an overall negative value during the observation period. The study area therefore served as a sink for atmospheric CO_2. In particular, the largest negative value (largest atmospheric CO_2 sink) in our study area was near the ice-edge south of 67°S (Fig. 7d).

3.3. Temporal variation of chl.a concentration

Temporal satellite images of the chl. *a* concentration near our sampling stations were shown in Figure 8. Prior to our sampling period (e.g. beginning of January), chl. *a* concentration at north-east area of our cruise track was high (up to 20 μg L^{-1}) (Fig. 8a). Then, chl. *a* concentration near our cruise track remained constant (around 0.2−5.0 μg L^{-1}) from middle to end of January 2009 (Figs. 8b−d).

4. Discussion

4.1. Influence of DSW outflow on DIC concentration

Dense water with low temperature and high DO was present on the ocean floor across the slope (Fig. 5) because DSW overflowed from the shelf as shelf water (SW) and became mSW, modified with mCDW (Hirano et al., 2015) (Fig. 1 and Table 1). Ohshima et al. (2013) have reported that Wild Canyon (corresponding to our study line) was the main route in the formation of AABW near the CDP (Fig. 2). Thus, the local

decrease in bottom DIC concentrations on the slope evident in vertical profiles and sections (e.g., Figs. 4d and 5d) was due to the overflow of SW formed from the mixing of low-temperature and dense DSW with low-DIC water from the shelf (Fig. 6). DSW kept its low DIC concentration with respect to the ambient mCDW, which had high DIC (Table 1), through the outflow process and formed AABW while mixing with mCDW (Fig. 1). This mSW also had relatively high DO. This helps to explain the low-temperature, high DO content, and dense water sinking from the surface to the deep layer along the slope.

The high DIC and low DO concentrations of CDW (origin of mCDW) have been described in past studies (e. g., Bakker et al., 2008; Roden et al., 2016). CDW—deep water long isolated from the surface—shows increases in DIC and decreases in DO because organic material from the surface layer sinks to the deep layer and is decomposed by bacteria. Thus, CDW has features of high DIC concentration and low DO (Bakker et al., 2008; Roden et al., 2016). In addition, as CDW rises and approaches Antarctica, CDW become mCDW due to cooling. Then, mCDW is transported to the sea-surface because the Southern Ocean near Antarctica is a divergence zone due to the Antarctic Circumpolar current and the Antarctic coastal current (Orsi et al., 1999). Around the coast, low DIC–high DO water forms through photosynthesis and dilution by sea-ice melt-water in summer (Fig. 1). Therefore, mCDW brought from the deep layer to the shelf is modified to low DIC-high DO water. The DIC concentration varies through mixing with ambient water and biological processes during transport, as explained above (Fig. 1).

4.2. Atmospheric CO_2 uptake in the CDP

The addition of freshwater to the surface water by melting of sea ice leads to a decrease in DIC concentration due to the dilution effect (e.g., Nomura et al., 2012). For example, Nomura et al. (2012) have reported that the decrease in salinity of 9.1 corresponded to the decrease in DIC of 565 μmol kg^{-1} in the surface water of the artificial pool (a square

pool with a dimension of 1.5 m × 1.5 m by cutting and removing the sea ice) during melting season. Near the coast, the dilution effect is further increased by the influx of glacier meltwater to the ocean, and surface ocean is stratified (Legge et al., 2017). Also, photosynthesis is known to be active in the polynyas and coastal areas of the Antarctic in summer (Arrigo and Van Dijken., 2003; Nomura et al., 2014). Arrigo and Van Dijken (2003) have reported that summer chl.*a* concentration increased to 2.2 μg L^{-1} in polynyas; our observed chl.*a* concentration of 5.1 μg L^{-1} at St. 7 exceeded that value. Satellite images of the chl. *a* concentration at north-east area of our cruise track was high (up to 20 μg L^{-1}) (Fig. 8a), and, chl. *a* concentration near our cruise track remained constant (around 0.2−5.0 μg L^{-1}) from middle to end of January 2009 (Figs. 8b−d). These results indicate that the CDP was also extremely productive in summer, with the dilution by meltwater contributing to the extreme decrease in $pCO_{2\ sea}$. As a result, the CDP had the potential to absorb large amounts of CO_2 from the atmosphere.

The literature to date for the Southern Ocean shows $pCO_{2\ sea}$ both supersaturated (Rubin et al., 1998; Metzl et al., 1999, 2006; Chierici et al., 2004; Inoue and Ishii, 2005; Nomura et al., 2014) and undersaturated (Bakker et al., 1997, 2008; Jabaud-Jan et al., 2004; Shim et al., 2006; Nomura et al., 2014; Legge et al., 2015; DeJong and Dunbar, 2017; Gray et al., 2018) relative to the atmosphere in spring and summer. However, in surface waters in polynyas likely affected by dilution and biological production, $pCO_{2\ sea}$ is undersaturated relative to the atmosphere in the summer (Shadwick et al., 2014; DeJong and Dunbar, 2017). The range of the $pCO_{2\ sea}$ observed in this study (172−362 μatm) and the very low $pCO_{2\ sea}$ were previously observed in this region (65−69°S, 60−72°E) for all cruises conducted in 1991 to 2017 (October−April, range 166−479 μatm, n=78557, see all pCO_2 data available in SOCAT, www.socat.info) (Bakker et al., 2016), and the lowest (166 μatm) and highest pCO_2 (479 μatm) were observed at middle of February and March, respectively. Temporal variation of SOCAT pCO_2 data indicated that mean pCO_2 decreased from October (382 μatm) to February (294 μatm) and increased from to April (362 μatm). The results confirm the well-known view, i.e. $pCO_{2\ sea}$ is low when chl. *a* concentration is high (e.g. Roden et al., 2016).

Sea−air CO_2 exchange depends on many parameters as shown in Eq. 2. However, the direction of gas flux (positive or negative) between the atmosphere and ocean is determined by $pCO_{2\ sea}$ saturation with respect to the atmosphere. Our estimate of CO_2 flux (average, −6.5 mmol C m^{-2} d^{-1}) falls within the values in the coast, sea ice zone, and polynya in spring and summer from past studies (average, from −41 to about 0 mmol C m^{-2} d^{-1}) (Gibson and Trull, 1999; Shadwick et al., 2014; Roden et al, 2016; DeJong and Dunbar, 2017; Gray et al., 2018, and references cited therein). Extremely higher negative fluxes were observed at the Terra Nova Bay in the western Ross Sea (−246 mmol C m^{-2} d^{-1}) and near Mawson station in Mac Robertson Land, East Antarctica (−221 mmol C m^{-2} d^{-1}) by the unique coupling of strong wind, low $pCO_{2\ sea}$, and minimal sea ice cover. Our largest negative value obtained near the ice-edge south of 67°S in CDP (−26.0 mmol C m^{-2} d^{-1}) is similar order of the value in the Mertz Polynya (−15 mmol C m^{-2} d^{-1}) (Shadwick et al., 2014). These results suggest, therefore, that the polynyas have high seasonal potential to absorb CO_2 from the atmosphere during the sampling period at least in the summer time.

4.3. Estimation of carbon transport associated with DSW outflow

The outflow of DSW formed in the CDP and formation of AABW raised the possibility that DSW was transported from the surface to the deep layer along with materials such as CO_2. At the same time, it was necessary to consider the processes that might compensate for DIC losses to deep water (mCDW). In this section we use a two-box model to quantitatively estimate net CO_2 (DIC) transport from the surface to deep layers in the CDP (Fig. 9). Given the oceanography in the CDP, we divided the SW and mCDW between the two boxes. In order to avoid the influence of dilution and brine addition on DIC concentrations, we use the DIC concentration normalized to salinity (nDIC; S = 34.25) for this discussion. The nDIC in SW and mCDW are expressed as C_{SW} (2212 ± 5 μmol kg^{-1}) and C_{mCDW} (2218 ± 11 μmol kg^{-1}), respectively.

DSW transport occurs mainly in wintertime (Ohshima et al., 2013). The T_{min} layer has been regarded as a proxy for chemical characteristic of the surface mixed layer in winter

(Ishii et al., 2002; Rubin et al., 1998; Hoppema and Goeyens, 1999; Pondaven et al., 2000; Nomura et al., 2014; Shadwick et al., 2014). Therefore, we used the nDIC concentration in the T_{min} layer (WW) for our estimation. On the shelf, however, the T_{min} layer was not well defined. Therefore, it was impossible for us to distinguish winter water from other water masses there (Table 1). Therefore, we decided to use the observed nDIC concentration at 100−200 m at St. 7 (C_{SW} = 2212 ± 5 μmol kg^{-1}) as the nDIC concentration in winter. Because this value was close to the average nDIC value (about 2211 μmol kg^{-1}) of the layer that could best be judged as winter water on the slope (T_{min} < −1.5 °C), we decided that it was appropriate to use the observed C_{SW} of 2212 ± 5 μmol kg^{-1}. Also, the seasonal change in nDIC concentration was shown to be small below a depth of about 100 m in the Mertz Polynya (Shadwick et al., 2014), supporting the representative of the seasonality on the shelf.

For the same period and line as our observations, the annual DSW ventilation rate in the CDP was estimated from mooring data to be 0.3−0.7 Sv (V_{MIX}) (Ohshima et al., 2013). We then used Eq. 3 to estimate the net annual DIC transport from the surface to the deep layer.

$$\Delta C_{total} = (C_{SW} - C_{mCDW})\, V_{MIX}\, \Delta T \qquad (3),$$

where ΔC_{total} is the net annual DIC transport from the surface to the deep layer, C_{SW} is mean nDIC in SW, C_{mCDW} is mean nDIC in mCDW, V_{MIX} is annual DSW ventilation rate in the CDP, and ΔT is time (a year). Because more nDIC flowed into SW from mCDW, with relatively higher nDIC concentration, the calculated ΔC_{total} was negative (-0.6×10^{11} to -1.4×10^{11} mol C). It has been demonstrated, however, that the subduction of DSW, rich in organic matter, is important for exporting anthropogenic CO_2 absorbed from the atmosphere to the deep layer (Shadwick et al., 2014, Bercovici et al. al., 2017).

4.4. Estimation of carbon consumption by primary production in the CDP using a two-box model

In the previous section, we examined the nDIC export process through the outflow of DSW. As a result, we calculated that 0.6×10^{11}–1.4×10^{11} mol C were added to SW annually. However, our observations showed that the summer nDIC concentration in SW remained low. DIC carried from mCDW onto the shelf therefore had to be consumed at 0.6×10^{11}–1.4×10^{11} mol C y^{-1} or released to the atmosphere as CO_2 gas and then returned to the deep layer with the low-nDIC DSW outflow. In winter in particular, $pCO_{2\,sea}$ is supersaturated compared to the atmosphere (e.g., Takahashi et al., 2009), and there is active CO_2 emission from the ocean to the atmosphere through open water. Alternatively, DIC concentrations are reduced through conversion to dissolved organic carbon (DOC) and particulate organic carbon (POC) via primary production in the coastal polynyas (Bercovici et al., 2017), and the carbon is then removed from SW as organic matter.

Satellite ocean color observations suggest that Antarctic coastal polynyas have a high productivity of 1.5–13.4 mol C m^{-2} y^{-1} (Arrigo and van Dijken, 2003), and this rate applied to the CDP area (14.3×10^9 m^2) yields 0.2×10^{11}–1.9×10^{11} mol C y^{-1}. In addition, Roden et al. (2016) have observed a high seasonally integrated net community production of up to 6.4 mol C m^{-2} off Cape Darnley (0.9×10^{11} mol C over the area of the CDP). Therefore, it could be inferred that the low nDIC concentration was maintained in the CDP through biological fixation of much of the nDIC supplied from the deep layer. We then used Eq. 4 to estimate the amount of organic matter ($\Delta C_{DOC/POC}$) converted from excess nDIC in the shelf water.

$$\Delta C_{DOC/POC} = \Delta C_{total} - \Delta C_{gas} \quad (4),$$

where ΔC_{total} is the excess nDIC in shelf water and ΔC_{gas} is the difference between the sea−air CO_2 flux in winter and summer ($F_{sea-air,\ winter} - F_{sea-air,\ summer}$). First, in order to obtain $F_{sea-air,\ winter}$, total alkalinity (TA) in winter (2324 μmol kg^{-1}) was evaluated using water temperature (−1.9 °C) and salinity (34.35 for WW). For calculation of TA, we used Eq. 5 from Lee et al. (2006).

$$TA = 2305+52.48\ (S-35)+2.85\ (S-35)^2-0.49\ (T-20)+0.086\ (T-20)^2 \qquad (5)$$

where S is the salinity (34.35) and T is the temperature (−1.9 °C). This equation was developed for the Southern Ocean (Lee et al., 2006).

Then, $pCO_{2\ sea}$ in winter (376 μatm) was calculated using calculated TA (2324 μmol kg^{-1}) and DIC (2212 μmol kg^{-1}) through CO_2 SYS, version 02.05 (Orr et al., 2018). From Eq. 2, we calculated $F_{sea-air,\ winter}$ as +0.2 mmol C m^{-2} d^{-1}. For this estimation, we used the mean wind speed of 6.5 m s^{-1} (Japan Meteorological Agency; http://www.data.jma.go.jp/obd/stats/etrn/index.php) and atmospheric CO_2 concentration of 383.3 ppmv (National Oceanic and Atmospheric Administration; https://www.esrl.noaa.gov/gmd/dv/iadv/) (pCO_2 of 372 μatm was calculated taking into account the saturated water vapor and atmospheric pressures) at Syowa station, East Antarctica for five months (from June to October 2009). In addition, it was assumed that 40% of the polynya was open water (=area of frazil ice) and that this flux lasted for five months in the polynya. For $F_{sea-air,\ summer}$, we assumed that the strong CO_2 sink (−25 mmol C m^{-2} d^{-1}) observed near the ice edge (see section 3.2) remained for at least a month. For the remaining six months, we assumed that the sum of $F_{sea-air}$ was zero. Given these assumptions, $F_{sea-air,\ winter}$, $F_{sea-air,\ summer}$ and ΔC_{gas} were 3.6×10^8 mol C, -1.1×10^{10} mol C, and -1.0×10^{10} mol C, respectively. Finally, we calculated $\Delta C_{DOC/POC}$ as 0.7×10^{11}–1.5×10^{11} mol C annually (Fig. 9).

Fang et al. (2018) have observed high DOC concentrations averaging about 20 μmol L^{-1} in DSW in the summer in Prydz Bay, East Antarctica. Therefore, we expected DSW to have a high DOC concentration even off Cape Darnley. These results indicate that part

of the DOC and POC produced over the shelf escapes through decomposition and is supplied to the deep layer through the DSW outflow in winter, and the supply of large amounts of DIC by the inflow of mCDW supports high biological production.

5. Conclusions

In this study we focused on carbonate chemistry in the CDP, East Antarctica. Figure 1 is a schematic illustration of the carbon cycle in the CDP. We have indicated the influences on the carbonate chemistry in the CDP associated with sea-ice production, the formation of dense water, and outflow to the deep ocean. During the period of our observations the ocean surface layer formed an intense CO_2 sink zone, absorbing on average 6.5 mmol C m^{-2} d^{-1}. The mSW overflowed the shelf and became AABW through mixing with mCDW with high DIC concentrations, although DIC concentrations in mSW remained lower than in surrounding water. Furthermore, we estimated the carbon flux related to primary production in the CDP by using a two-box model. DIC concentrations in surface water remained low over the shelf by the conversion of DIC supplied from the deep layer to organic matter through high biological production. We clarified the effect of the dense water formed by sea-ice formation on carbonate chemistry in the CDP.

6. Acknowledgments

We thank the crew of R/V *Umitaka Maru* and cruise members for their support in conducting the field work. We greatly benefitted from advice offered by Shuki Uhio, Takeshi Tamura, Shintaro Takao, Yasushi Fukamachi, Shigeru Aoki, Atsushi Ooki, and Akihide Kasai, and from their useful comments about this paper. This work was supported by grants from the Japan Society for the Promotion of Science (#20221001 and #17H04715), the Joint Research Program of the Institute of Low Temperature Science, Hokkaido University (#18G038) and the National Institute for Polar Research

(#28-14). The pCO_2 data in this study are available in SOCAT data-base (www.socat.info).

References

Arrigo, K. R., and G. L. van Dijken (2003). Phytoplankton dynamics within 37 Antarctic coastal polynya systems. *Journal of Geophysical Research*, 108(C8), 3271, doi:10.1029/2002JC001739.

Bakker, D. C. E., H. J. W. de Baar, and U. V. Bathmann (1997). Changes of carbon dioxide in surface waters during spring in the Southern Ocean. *Deep-Sea Research*. II, 44, 91–127.

Bakker, D. C. E., Hoppema, M., Schröder, M., Geibert, W., and de Baar, H. J. W. (2008). A rapid transition from ice covered CO_2-rich waters to a biologically mediated CO2 sink in the eastern Weddell Gyre. *Biogeosciences*, 5, 1373–1386, doi:10.5194/bg-5-1373-2008.

Bakker, D. C. E., Pfeil, B., Landa, C. S., Metzl, N., O'Brien, K. M., Olsen, A., et al. (2016). A multi-decade record of high-quality fCO_2 data in version 3 of the Surface Ocean CO2 Atlas (SOCAT). *Earth System Science Data*, 8(2), 383-413. https://doi.org/10.5194/essd-8-383-2016.

Bercovici, S. K., Huber, B. A., DeJong, H. B., Dunbar, R. B., and Hansell, D. A. (2017). Dissolved organic carbon in the Ross Sea: Deep enrichment and export. *Limnology and Oceanography*, https://doi.org/10.1002/lno.10592.

Chierici, M., Fransson, A., Turner, D. R., Pakhomov, E. A., and Froneman, P. W. (2004). Variability in pH, fCO2, oxygen and flux of CO2 in the surface water along a transect in the Atlantic sector of the Southern Ocean. *Deep Sea Research Part II: Topical Studies in Oceanography*, *51*(22–24), 2773–2787, doi:10.1016/j.dsr2.2001.03.002.

Comiso, J. C. (2010). Variability and trends of the global sea ice cover. *Sea ice*, *2*, 205–246.

Copin-Montegut, C. (1988). A new formula for the effect of temperature on the partial pressure of CO_2 in seawater, *Marine Chemistry, 25*, 29–37, 1988 (Correction, *Marine Chemistry*, *27,* 143–144, 1989).

DeJong, H. B., and Dunbar, R. B. (2017). Air-sea CO2 exchange in the Ross Sea, Antarctica. *Journal of Geophysical Research: Oceans*, 122. https://doi.org/10.1002/2017JC012853.

Fang, Z., Yang, W., Chen, M., Stubbins, A., Ma, H., Jia, R., et al (2018). Transport of dissolved black carbon from the Prydz Bay Shelf, Antarctica to the deep Southern Ocean. *Limnology and Oceanography*, *63*(5), 2179–2190, doi:10.1002/lno.10932.

Gibson, J. A. E., and Trull, T. W. (1999). Annual cycle of fCO_2 under sea-ice and in open water in Prydz Bay, East Antarctica. *Marine Chemistry*, 66(3–4), 187–200. https://doi.org/10.1016/S0304-4203(99)00040-7.

Gray, A., Johnson, K. S., Bushinsky, S. M., Riser, S. C., Russell, J. L., Talley, L. D., et al. (2018). Autonomous biogeochemical floats detect significant carbon dioxide outgassing in the high-latitude Southern Ocean. *Geophysical Research Letters*, 45, 9049–9057. https://doi.org/10.1029/2018GL078013.

Hirano, D., Kitade, Y., Ohshima, K. I., and Fukamachi, Y. (2015). The role of turbulent mixing in the modified Shelf Water overflows that produce Cape Darnley Bottom Water. *Journal of Geophysical Research: Oceans*, *120*(2), 910–922, doi:10.1002/2014JC010059.

Hoppema, M., and Goeyens, L. (1999). Redfield behavior of carbon, nitrogen, and phosphorus depletions in Antarctic surface water. *Limnology and Oceanography*, *44*(1),

220–224, doi:10.4319/lo.1999.44.1.0220.

Inoue, H. Y. and Ishii, M.(2005). Variations and trends of CO_2 in the surface seawater in the Southern Ocean south of Australia between 1969 and 2002, *Tellus B*, 58–69.

Ishii, M., Inoue, H. Y., and Matsueda, H. (2002). Net community production in the marginal ice zone and its importance for the variability of the oceanic pCO2 in the Southern Ocean south of Australia. *Deep Sea Research Part II: Topical Studies in Oceanography*, *49*(9–10), 1691–1706, doi.org/10.1016/S0967-0645(02)00007-3.

Jabaud-Jan, A., Metzl, N., Brunet, C., Poisson, A., and Schauer, B. (2004). Interannual variability of the carbon dioxide system in the southern Indian Ocean (20 S–60 S): The impact of a warm anomaly in austral summer 1998. *Global Biogeochemical Cycles*, *18*(1), doi:10.1029/2002GB002017, 2.

Jackett, D. R., and McDougall, T. J. (1997). A neutral density variable for the world's oceans. *Journal of Physical Oceanography*, *27*(2), 237–263, doi.org/10.1175/1520-0485(1997)027<0237:ANDVFT>2.0.CO;2.

Johnson, K. M. (1992). "Operator's Manual: Single-Operator Multiparameter Metabolic Analyzer (SOMMA) for Total Carbon Dioxide (CT) with Coulometric Detection." Brookhaven National Laboratory, Brookhaven, NY.

Landschützer, P., Gruber, N., Haumann, F. A., Rödenbeck, C., Bakker, D. C. E., van Heuven, S., Hoppema, M., Metzl, N., Sweeney, C., Takahashi, T., Tilbrook, B. and Wanninkhof, R.: The reinvigoration of the Southern Ocean carbon sink, *Science*, 349(6253), 1221, doi:10.1126/science.aab2620, 2015.

Lee, K., Tong, L. T., Millero, F. J., Sabine, C. L., Dickson, A. G., Goyet, C., et al (2006). Global relationships of total alkalinity with salinity and temperature in surface waters of the world's oceans. *Geophysical research letters*, *33*(19), doi:10.1029/2006GL027207.

Legge, O. J., D. C. E.Bakker, M. T. Johnson, M. P. Meredith, H. J. Venables, P. J. Brown, and G. A. Lee (2015). The seasonal cycle of ocean-atmosphere CO2 flux in Ryder Bay, west Antarctic Peninsula, *Geophysical research letters*, 42, 2934–2942, doi:10.1002/2015GL063796.

Legge, O. J., Bakker, D. C., Meredith, M. P., Venables, H. J., Brown, P. J., Jones, E. M., and Johnson, M. T. (2017). The seasonal cycle of carbonate system processes in Ryder Bay, West Antarctic Peninsula. *Deep Sea Research Part II: Topical Studies in Oceanography*, *139*, 167–180, doi.org/10.1016/j.dsr2.2016.11.006.

Lenton, A., B. Tilbrook, R. M. Law, D. Bakker, S. C. Doney, N. Gruber, M.Ishii, M. Hoppema, N. S. Lovenduski, R. J. Matear, B. I. McNeil, N. Metzl, S. E. Mikaloff Fletcher, P. M. S. Monteiro, C. Rödenbeck, C. Sweeney, and T. Takahashi. (2013). Sea--air CO_2 fluxes in the Southern Ocean for the period 1990-2009. Biogeosciences, 10, 4037-4054, doi:10.5194/bg-10-4037-2013.

Metzl, N., Tilbrook, B., and Poisson, A. (1999). The annual fCO2 cycle and the air-sea CO2 flux in the sub-Antarctic Ocean. *Tellus B: Chemical and Physical Meteorology*, *51*(4), 849–861, doi.org/10.3402/tellusb.v51i4.16495.

Metzl, N., Brunet, C., Jabaud-Jan, A., Poisson, A., and Schauer, B. (2006). Summer and winter air–sea CO2 fluxes in the Southern Ocean. *Deep Sea Research Part I: Oceanographic Research Papers*, *53*(9), 1548–1563, doi:10.1016/j.dsr.2006.07.006.

Nakaoka, S., Nakazawa, T., Yoshikawa-Inoue, H., Aoki, S., Hashida, G., Ishii, M., Yamanouchi, T., Odate, T., and Fukuchi, M. (2009). Summertime variations of oceanic pCO2 and air-sea CO2 flux in the eastern Indian sector of the Southern Ocean, Geophys. Res. Lett. 36, L14610, doi:10.1029/2009GL038467.

Nomura, D., Yoshikawa-Inoue, H., and Toyota, T. (2006). The effect of sea-ice growth on air–sea CO2 flux in a tank experiment. *Tellus B: Chemical and Physical*

Meteorology, *58*(5), 418–426, doi.org/10.1111/j.1600-0889.2006.00204.x.

Nomura, D., Simizu, D., Chavanich, S., Shinagawa, H., and Fukuchi, M. (2012). An artificial pool experiment in Antarctic sea ice: effects of sea ice melting on physical and biogeochemical components of pool water. *Antarctic Science*, *24*(5), 536–544, doi:10.1017/S0954102012000284.

Nomura, D., Yoshikawa-Inoue, H., Kobayashi, S., Nakaoka, S., Nakata, K., and Hashida, G. (2014). Winter-to-summer evolution of pCO_2 in surface water and air–sea CO_2 flux in the seasonal ice zone of the Southern Ocean. *Biogeosciences*, *11*(20), 5749–5761, doi.org/10.5194/bg-11-5749-2014.

Ohshima, K. I., Fukamachi, Y., Williams, G. D., Nihashi, S., Roquet, F., Kitade, Y., et al. (2013). Antarctic Bottom Water production by intense sea-ice formation in the Cape Darnley polynya. *Nature Geoscience*, *6*(3), 235, DOI: 10.1038/NGEO1738.

O'Reilly, J.E., & 24 co-authors (2000). SeaWiFS Postlaunch Calibration and Validation Analyses, Part 3. NASA Tech. Memo. 2000-206892, Vol. 11, S.B. Hooker and E.R. Firestone, Eds., NASA Goddard Space Flight Center, 49 pp.

Orr, J. C., Epitalon, J.-M., Dickson, A. G., & Gattuso, J.-P. (2018). Routine uncertainty propagation for the marine carbon dioxide system. *Marine Chemistry*, 207, 84–107. https://doi.org/10.1016/j.marchem.2018.10.006.

Orsi, A. H., and Wiederwohl, C. L. (2009). A recount of Ross Sea waters. *Deep Sea Research Part II: Topical Studies in Oceanography*, *56*(13–14), 778–795, doi:10.1016/j.dsr2.2008.10.033.

Orsi, A. H., Johnson, G. C., and Bullister, J. L. (1999). Circulation, mixing, and production of Antarctic Bottom Water. *Progress in Oceanography*, *43*(1), 55–109.

Pondaven, P., Ragueneau, O., Treguer, P., Hauvespre, A., Dezileau, L., and Reyss, J. L.

(2000). Resolving the ‘opal paradox’in the Southern Ocean. *Nature*, *405*(6783), 168.

Roden, N. P., Tilbrook, B., Trull, T. W., Virtue, P., and Williams, G. D. (2016). Carbon cycling dynamics in the seasonal sea‐ice zone of East Antarctica. *Journal of Geophysical Research: Oceans*, *121*(12), 8749–8769, doi:10.1002/ 2016JC012008.

Rubin, S. I., Takahashi, T., Chipman, D. W., and Goddard, J. G. (1998). Primary productivity and nutrient utilization ratios in the Pacific sector of the Southern Ocean based on seasonal changes in seawater chemistry. *Deep sea research part I: Oceanographic Research Papers*, *45*(8), 1211–1234, doi.org/10.1016/S0967-0637(98)00021-1.

Rysgaard, S., Glud, R. N., Sejr, M. K., Bendtsen, J., and Christensen, P. B. (2007). Inorganic carbon transport during sea ice growth and decay: A carbon pump in polar seas. *Journal of Geophysical Research: Oceans*, *112*(C3), doi:10.1029/2006JC003572.

Sabine, C. L., Feely, R. A., Gruber, N., Key, R. M., Lee, K., Bullister, J. L., et al. (2004). The oceanic sink for anthropogenic CO2. *science*, *305*(5682), 367–371, DOI: 10.1126/science.1097403.

Sallée, J. B., Matear, R. J., Rintoul, S. R., and Lenton, A. (2012). Localized subduction of anthropogenic carbon dioxide in the Southern Hemisphere oceans. *Nature Geoscience*, *5*(8), 579–584, DOI: 10.1038/NGEO1523.

Shadwick, E. H., Tilbrook, B., and Williams, G. D. (2014). Carbonate chemistry in the Mertz Polynya (East Antarctica): Biological and physical modification of dense water outflows and the export of anthropogenic CO2. *Journal of Geophysical Research: Oceans*, *119*(1), 1–14., doi:10.1002/2013JC009286.

Shim, J., Kang, Y. C., Kim, D., and Choi, S. H. (2006). Distribution of net community production and surface pCO2 in the Scotia Sea, Antarctica, during austral spring

2001'. *Marine chemistry*, *101*(1–2), 68–84, doi.org/10.1016/j.marchem.2005.12.007.

Strickland, J.D.H. and Parsons, T.R. (1968). A practical handbook of seawater analysis. *Journal of the Fisheries Research Board of Canada*., Ottawa, 311 pages.

Suzuki, R., and Ishimaru, T. (1990). An improved method for the determination of phytoplankton chlorophyll using N,N-dimethylformamide. *Journal of the Oceanographic Society of Japan*, *46*, 190–194. https://doi.org/10.1007/BF02125580.

Takahashi, T., Sutherland, S. C., Wanninkhof, R., Sweeney, C., Feely, R. A., Chipman, D. W., et al (2009). Climatological mean and decadal change in surface ocean pCO2, and net sea–air CO2 flux over the global oceans. *Deep Sea Research Part II: Topical Studies in Oceanography*, *56*(8–10), 554–577, doi:10.1016/j.dsr2.2008.12.009.

Takahashi, T., Sweeney, C., Hales, B., Chipman, D. W., Newberger, T., Goddard, J. G., et al. (2012). The changing carbon cycle in the Southern Ocean. *Oceanography*, *25*(3), 26–37, doi:10.1016/j.dsr2.2008.12.009.

Tamura, T., Ohshima, K. I., and Nihashi, S. (2008). Mapping of sea ice production for Antarctic coastal polynyas. *Geophysical Research Letters*, *35*(7), doi:10.1029/2007GL032903, 2008.

Wakatsuchi, M., and Ono, N. (1983). Measurements of salinity and volume of brine excluded from growing sea ice. *Journal of Geophysical Research: Oceans*, *88*(C5), 2943–2951, doi.org/10.1029/JC088iC05p02943.

Wanninkhof, R.H., Park, G.-H., Takahashi, T., Sweeney, C., Feely, R., Nojiri, Y., et al. (2013). Global ocean carbon uptake: magnitude, variability and trends. Biogeosciences, 10(3), 1983–2000. https://doi.org/10.5194/bg-10-1983-2013

Weiss, R. (1974). Carbon dioxide in water and seawater: the solubility of a non-ideal gas. *Marine chemistry*, *2*(3), 203–215.

Williams, G. D., Herraiz-Borreguero, L., Roquet, F., Tamura, T., Ohshima, K. I., Fukamachi, Y., Fraser, A. D., Gao, L., Chen, H., McMahon, C. R., Harcourt, R. and Hindell, M. (2016). The suppression of Antarctic bottom water formation by melting ice shelves in Prydz Bay, *Nature Communications*, 7, 12577, doi:10.1038/ncomms12577.

Figure captions

Figure 1. Schematic illustration of the water mass and carbon cycle near the Cape Darnley polynya.

Figure 2. Location map of the sampling area near Cape Darnley, East Antarctica, showing CTD stations. The pink line indicates the area of the Cape Darnley polynya, which is defined as a high ice-production area with an annual ice production >5 m (Ohshima et al., 2013). The blue line indicates the cruise track. Images derived from AMSR-E satellite data.

Figure 3. Relationship between observed DIC concentrations (DIC_{obs}) and those calculated using multiple linear regression (DIC_{MLR}). Dotted line shows the regression line for this relationship. DIC_{obs} used in this figure were collected vertically (>100 m) from Sts. 1−6.

Figure 4. Vertical profiles of (a) potential temperature, (b) salinity, (c) dissolved oxygen, and (d) DIC concentrations (line: DIC_{MLR} and circle: DIC_{obs}) at St. 3 off Cape Darnley, East Antarctica. DIC_{MLR} was indicated for >100 m.

Figure 5. Vertical sections of (a) potential temperature, (b) salinity, (c) dissolved oxygen, and (d) DIC concentrations (DIC_{MLR}) from St. 1 to St. 6 near Cape Darnley, East Antarctica. Dashed lines indicate neutral density layers of 28.0 and 28.27, and the neutral density between 28.0 and 28.27 with $\theta \leqq +1.5$ °C is mCDW.

Figure 6. DIC concentrations (DIC_{obs}) at the bottom and 100 m above the bottom for each station.

Figure 7. Sea surface (a) temperature (SST), (b) salinity (SSS), (c) $pCO_{2\ sea}$ as measured by the underway water pumping system onboard the R/V *Umitaka Maru*, and (d) sea−air CO_2 flux.

Figure 8. Temporal variation in chl.*a* concentration in the study area for 1–8 (a), 9–16 (b), 17–24 January (c) and 25 January–1 February 2009 (d) from MODIS imagery. The white line indicates the cruise track.

Figure 9. Schematic illustration of a two-box model for modified Circumpolar Deep Water (mCDW) and Shelf Water (SW) near Cape Darnley, East Antarctica. Both mCDW and SW boxes are assumed to be homogeneous. Biological uptake of inorganic constituents in the SW box reduces the DIC concentration (C_{sw}) and removes DIC as POC and DOC ($\Phi_{DOC/POC}$). The CO_2 flux between SW and atmosphere ($\Phi_{CO2\ flux}$) changes C_{sw}. The two boxes exchange water at a volume rate equal to V_{mix}.

Table caption

Table 1. Definition, subcategories, neutral density (γ^n), potential temperature (θ), salinity, and DIC concentration for each water mass in the study area. Water masses were defined by neutral density (γ^n) (Jackett and McDougal, 1997) based on Orsi and Wiederwohl (2009) and Roden et al. (2016). The observed mean and standard deviation are shown for each parameter. AASW, CDW, Circumpolar Deep Water; Antarctic Surface Water; mCDW, modified Circumpolar Deep Water; AABW, Antarctic Bottom Water; SW, Shelf Water; mSW, modified Shelf Water. Roden et al. (2016) defined the mSW shallower than 2500 m while we defined shallower than 2000 m. Therefore, DIC of mSW in Roden et al. (2016) was higher (2257 μmol kg^{-1}) than that in our study

because DIC concentration in the deep ocean is high. There was no CDW and SW in our study area.

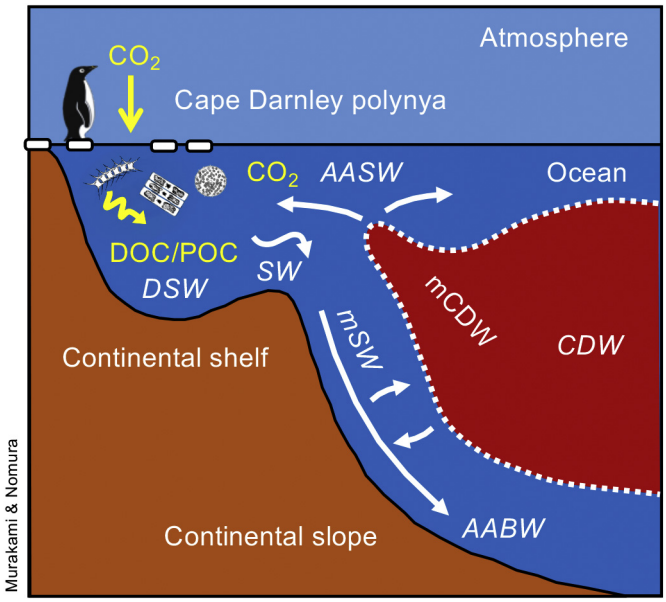
Atmosphere
CO_2
Cape Darnley polynya
CO_2
AASW
Ocean
DOC/POC
DSW
SW
mCDW
CDW
mSW
Continental shelf
Continental slope
AABW
Murakami & Nomura

Figure 1

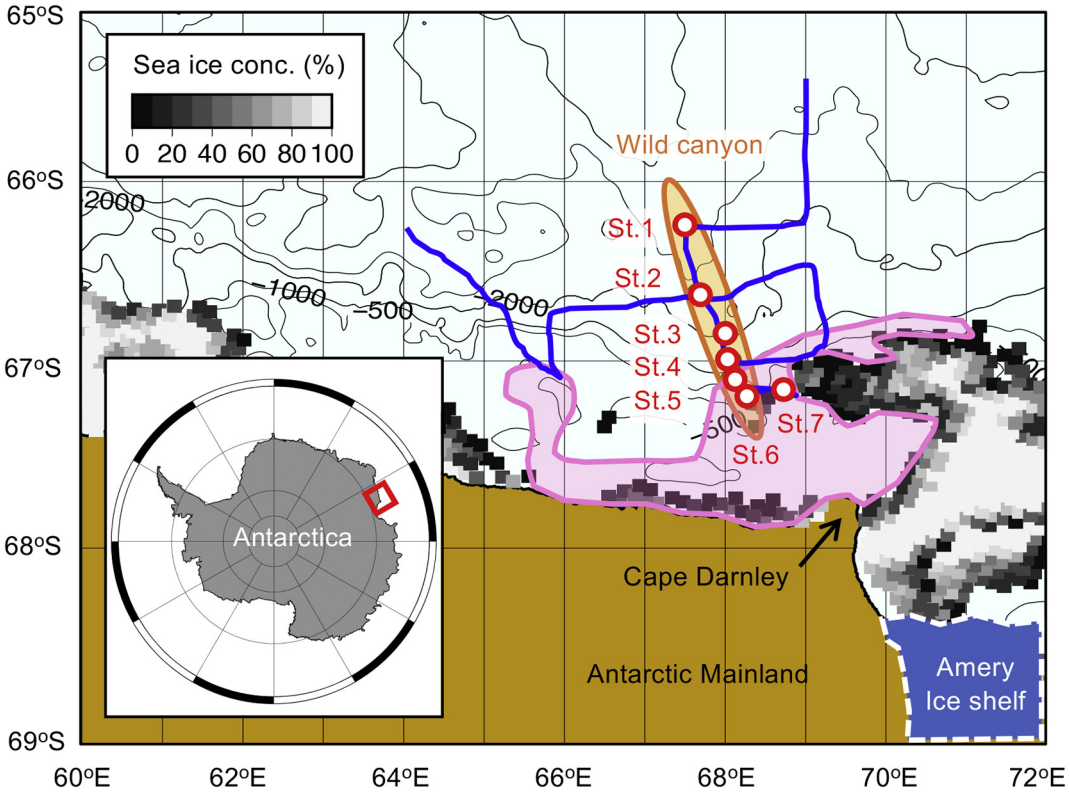
Sea ice conc. (%)
0 20 40 60 80 100
Wild canyon
St.1
St.2
St.3
St.4
St.5
St.6
St.7
2000
1000
500
Antarctica
Cape Darnley
Antarctic Mainland
Amery
Ice shelf
65°S
66°S
67°S
68°S
69°S
60°E
62°E
64°E
66°E
68°E
70°E
72°E

Figure 2

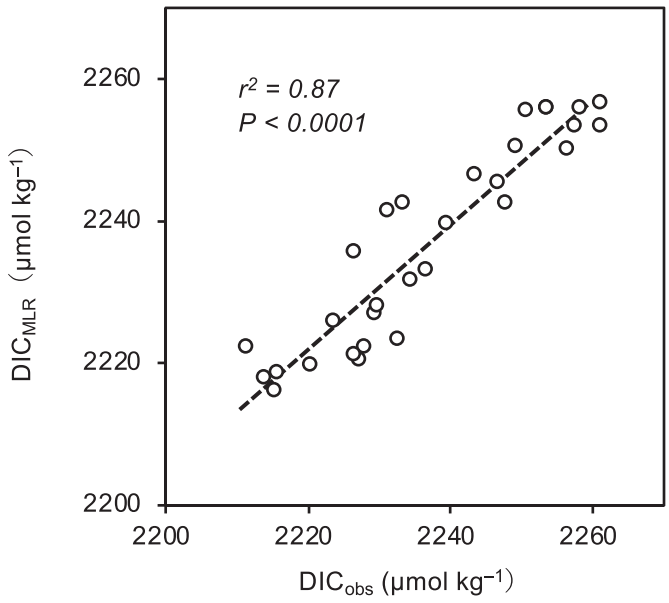
r^2 = 0.87
P < 0.0001
2260
2240
2220
2200
2200
2220
2240
2260
DIC_{MLR} (μmol kg^{-1})
DIC_{obs} (μmol kg^{-1})

Figure 3

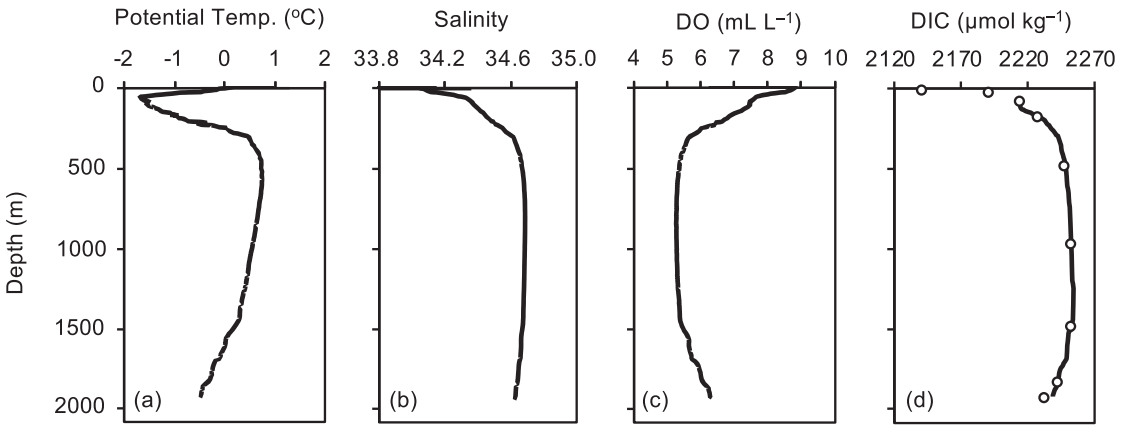
Potential Temp. (°C)
-2 -1 0 1 2
Salinity
33.8 34.2 34.6 35.0
DO (mL L⁻¹)
4 5 6 7 8 9 10
DIC (µmol kg⁻¹)
2120 2170 2220 2270
Depth (m)
0
500
1000
1500
2000
(a)
(b)
(c)
(d)

Figure 4

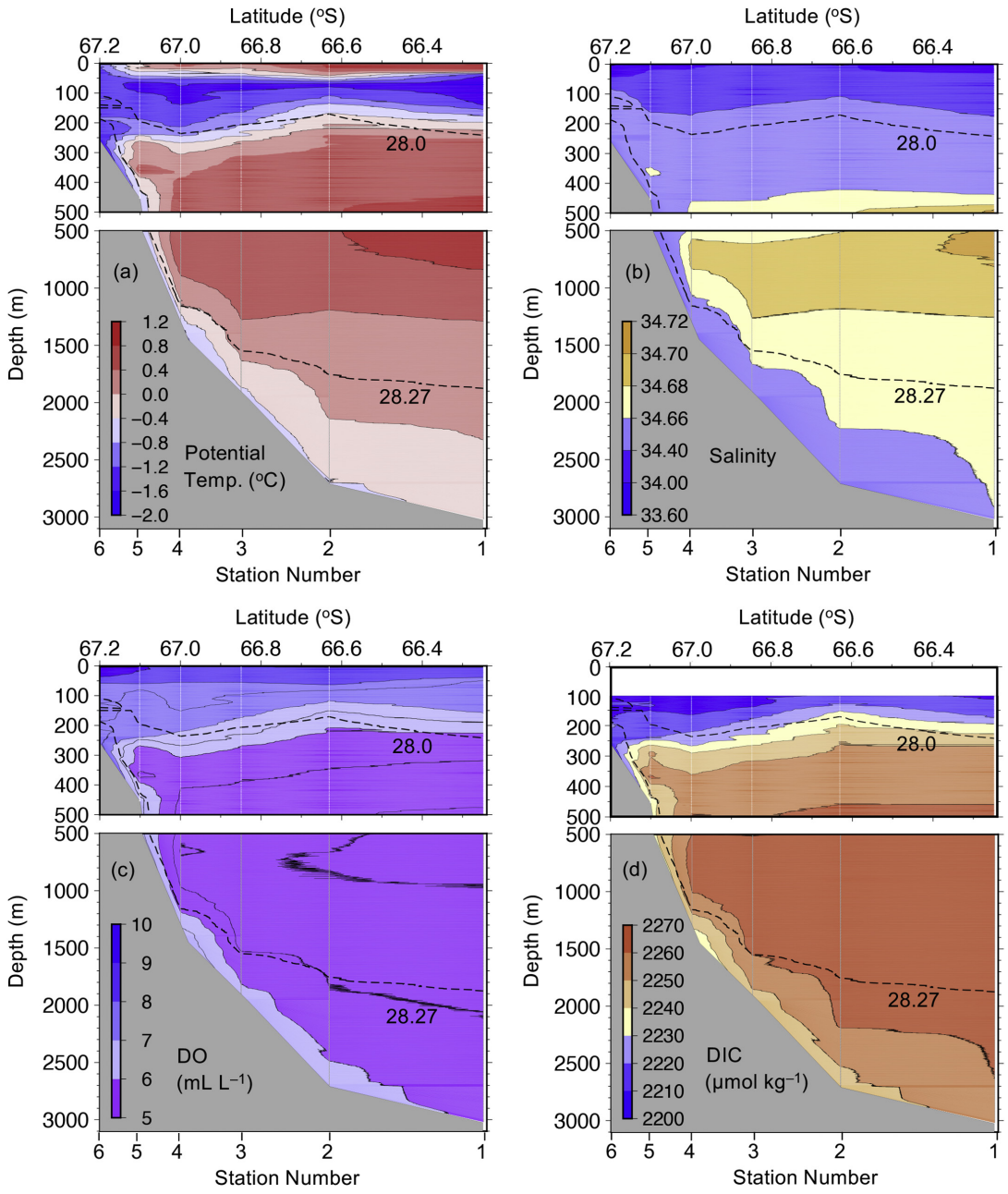
Latitude (°S)
67.2
67.0
66.8
66.6
66.4
28.0
28.27
(a)
Potential
Temp. (°C)
1.2
0.8
0.4
0.0
−0.4
−0.8
−1.2
−1.6
−2.0
(b)
Salinity
34.72
34.70
34.68
34.66
34.40
34.00
33.60
(c)
DO
(mL L⁻¹)
10
9
8
7
6
5
(d)
DIC
(μmol kg⁻¹)
2270
2260
2250
2240
2230
2220
2210
2200
Depth (m)
Station Number
6
5
4
3
2
1

Figure 5

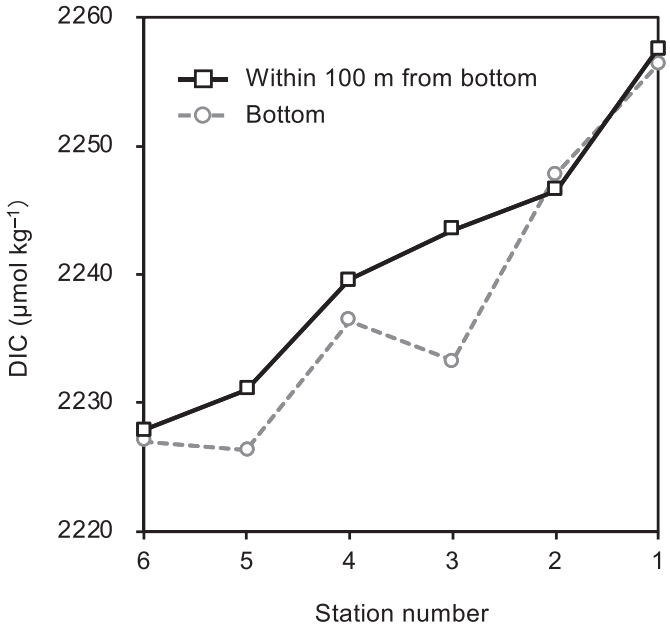
2260
2250
2240
2230
2220
DIC (μmol kg⁻¹)
Within 100 m from bottom
Bottom
6
5
4
3
2
1
Station number

Figure 6

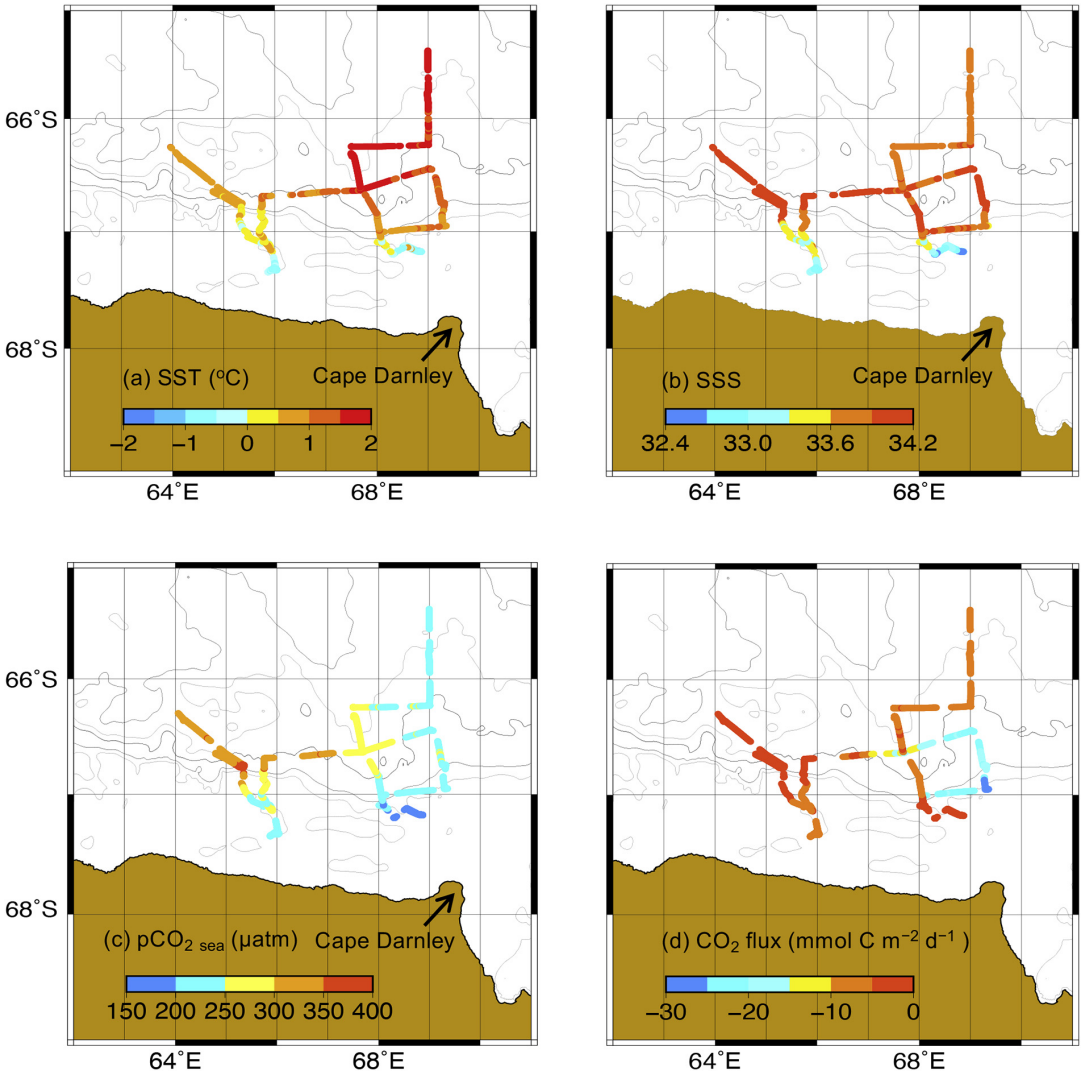
66°S
68°S
(a) SST (°C)
Cape Darnley
−2 −1 0 1 2
64°E
68°E
(b) SSS
Cape Darnley
32.4 33.0 33.6 34.2
64°E
68°E
66°S
68°S
(c) pCO2 sea (µatm)
Cape Darnley
150 200 250 300 350 400
64°E
68°E
(d) CO2 flux (mmol C m−2 d−1)
−30 −20 −10 0
64°E
68°E

Figure 7

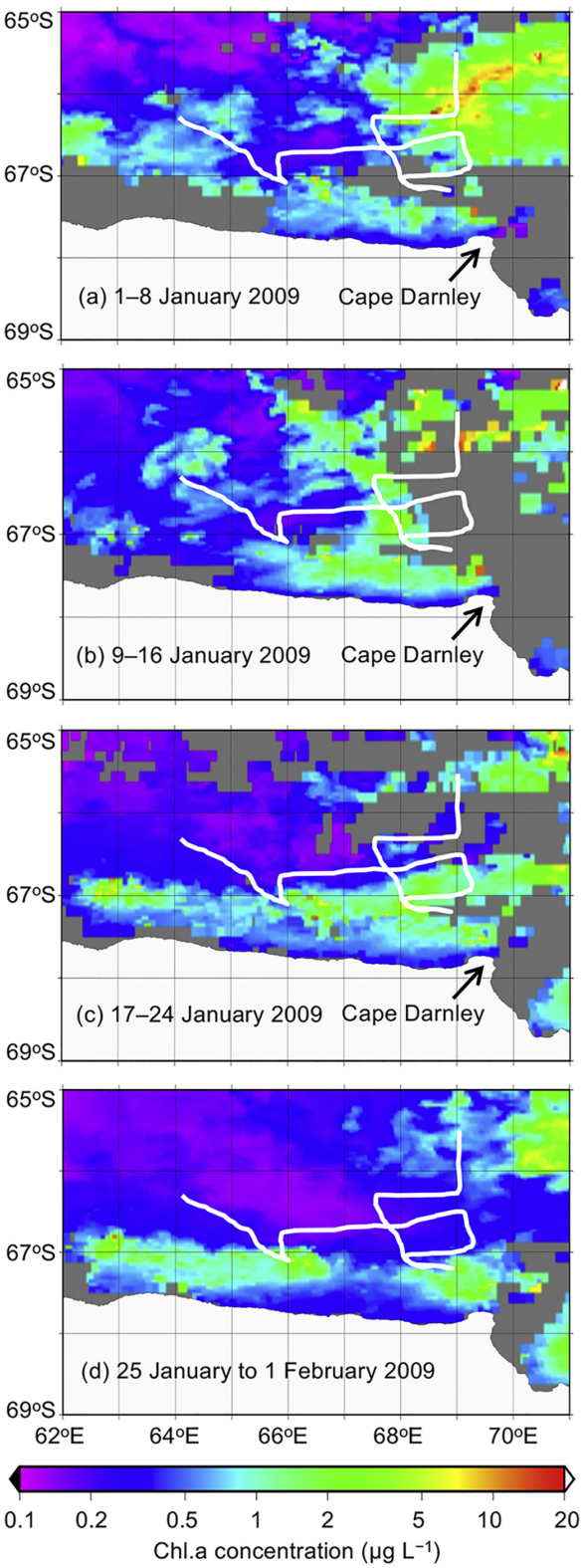
65°S
67°S
69°S
(a) 1–8 January 2009
Cape Darnley
(b) 9–16 January 2009
Cape Darnley
(c) 17–24 January 2009
Cape Darnley
(d) 25 January to 1 February 2009
62°E
64°E
66°E
68°E
70°E
0.1
0.2
0.5
1
2
5
10
20
Chl.a concentration (µg L⁻¹)

Figure 8

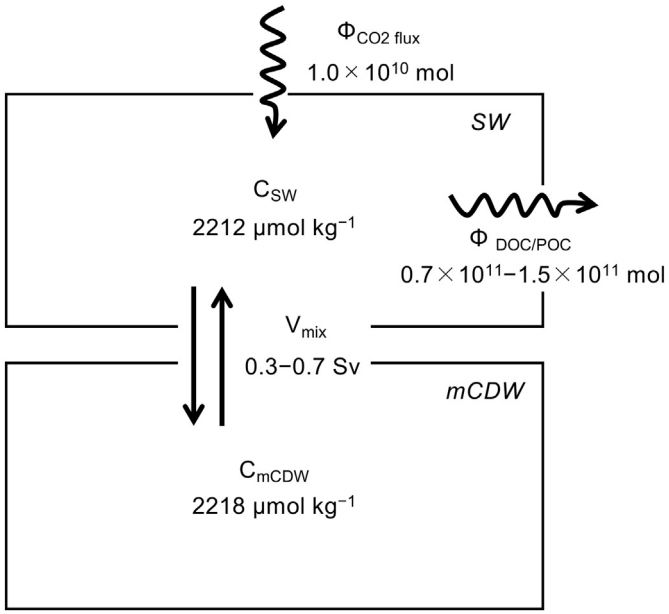
$\Phi_{CO2\ flux}$
1.0×10^{10} mol
SW
C_{SW}
2212 μmol kg^{-1}
$\Phi_{DOC/POC}$
0.7×10^{11}–1.5×10^{11} mol
V_{mix}
0.3–0.7 Sv
mCDW
C_{mCDW}
2218 μmol kg^{-1}

Figure 9

Table 1

Water mass	Definitions and subcategories	γ^n	θ (°C)	Salinity	DIC (μmol kg^{-1})
AASW	$\gamma^n < 28.00$	27.80 ± 0.23	−1.05 ± 0.67	34.26 ± 0.23	2161 ± 64
CDW	$28.00 \leqq \gamma^n \leqq 28.27$ $\theta > 1.5$ °C	–	–	–	–
mCDW	$28.00 \leqq \gamma^n \leqq 28.27$ $\theta \leqq 1.5$ °C	28.17 ± 0.07	+0.40 ± 0.47	34.66 ± 0.05	2241 ± 16
AABW	$\gamma^n > 28.27$ Depth > 2000 m	28.31 ± 0.02	−0.10 ± 0.14	34.66 ± 0.01	2253 ± 5
SW	$\gamma^n > 28.27$ (Slope) $\theta \leqq -1.85$ °C	–	–	–	–
mSW	$\gamma^n > 28.27$ (Slope) $\theta > -1.85$ °C	28.34 ± 0.04	−0.76 ± 0.39	34.60 ± 0.03	2230 ± 5